Archives of Biochemistry and Biophysics 761 (2024) 110181

Contents lists available at ScienceDirect

Archives of Biochemistry and Biophysics

journal homepage: www.elsevier.com/locate/yabbi

Interactions of novel 1,3-diaryltriazene-sulfamethazines with carbonic anhydrases: Kinetic studies and *in silico* simulations

Nabih Lolak [a], Cüneyt Türkeş [b,*], Suleyman Akocak [a,**], Hatice Esra Duran [c], Mesut Işık [d], Mustafa Durgun [e], Şükrü Beydemir [f]

[a] Department of Pharmaceutical Chemistry, Faculty of Pharmacy, Adıyaman University, Adıyaman, 02040, Turkey
[b] Department of Biochemistry, Faculty of Pharmacy, Erzincan Binali Yıldırım University, Erzincan, 24002, Turkey
[c] Department of Medical Biochemistry, Faculty of Medicine, Kafkas University, Kars, 36100, Turkey
[d] Department of Bioengineering, Faculty of Engineering, Bilecik Şeyh Edebali University, Bilecik, 11230, Turkey
[e] Department of Chemistry, Faculty of Arts and Sciences, Harran University, Şanlıurfa, 63290, Turkey
[f] Department of Biochemistry, Faculty of Pharmacy, Anadolu University, Eskişehir, 26470, Turkey

ARTICLE INFO

Keywords:
Carbonic anhydrase
Triazene
Sulphamethazine
Selective inhibitor
In silico study

ABSTRACT

Sulfonamides, recognized as carbonic anhydrase (CA, EC 4.2.1.1) inhibitors, are crucial in treating diverse diseases, including epilepsy, glaucoma, bacterial infections, and various pathological processes, e.g., high blood pressure, rheumatoid arthritis, ulcerative colitis, pain, and inflammation. Additionally, therapeutically, 1,3-diaryl-substituted triazenes and sulphamethazines (**SM**) are integral components in various drug structures, and the synthesis of novel compounds within these two categories holds substantial significance. Herein, ten 1,3-diaryltriazene-substituted sulphamethazine derivatives **SM(1–10)**, which were created by reacting the diazonium salt of sulphamethazine with substituted aromatic amines, were synthesized and the physiologically and pharmacologically relevant human (*h*) isoforms *h*CA I and II, cytosolic isozymes, were included in the study. The synthesized compounds showed excellent inhibition versus *h*CAs; the 4-butoxy (**SM7**, K_I of 5.69 ± 0.59 nM) compound exhibited a potent inhibitory effect against the *h*CA I compared with the reference drug acetazolamide (AAZ, K_I of 116.00 ± 8.48 nM). The 4-cyano (**SM4**, K_I of 5.87 ± 0.57 nM) compound displayed higher potency than AAZ (K_I of 57.25 ± 4.15 nM) towards *h*CA II. Meanwhile, among the synthesized molecules, the 3,4-dimethoxy (**SM9**, K_I of 74.98 ± 10.49 nM, S_I of 9.94) compound (over *h*CA I) displayed a noticeable selectivity for *h*CA isoform II. The target compounds in the molecular docking investigation were determined to take part in various hydrophilic and hydrophobic interactions with nearby amino acids and fit nicely into the active sites of the *h*CAs. This research has yielded compounds displaying varying affinity toward *h*CA isoenzymes, ultimately serving as potent and selective *h*CA inhibitors. Given its substantial biological inhibitory potency, this particular derivative series is determined to hold the potential to serve as a promising lead compound against these *h*CAs.

1. Introduction

Carbonic anhydrases (CAs; EC 4.2.1.1) [1] are a group of enzyme isoforms found throughout the animal kingdom [2], exhibiting diverse physiological and biochemical functions [3]. Numerous critical physiological and pathological processes [4], such as pH homeostasis [5], gluconeogenesis [6], fluid secretion [7], bone resorption [8], and tumorgenicity [9], depend on these pervasive metalloenzymes, which catalyze the reversible conversion of water and CO_2 to HCO_3^- and H^+ [10]. A total of fifteen different isozymes [11], including cytosolic (I, II, III, VII, and XIII) [12], membrane-bound (IV, IX, XII, and XIV) [13], secreted (VI) [14], and mitochondrial (VA and VB) [15] isozymes, have been found in the human CA isoforms (hCA), which are extensively distributed in different tissues [16]. *h*CA II, one of the most widely studied isoforms [17], exhibits the highest turnover rate among all *h*CAs, with a k_{cat} of 10^6 s^{-1} [18]. The enzyme has an exceptionally high turnover rate because of the quick proton transfer made possible by the proximity of the His 64 residue to the active site [19]. Given its critical role in the primary transport pathway of sodium into the eye [20], *h*CA II is responsible for regulating intraocular pressure [21], which is

* Corresponding author.
** Corresponding author.
E-mail addresses: cuneyt.turkes@erzincan.edu.tr (C. Türkeş), sakocak@adiyaman.edu.tr (S. Akocak).

https://doi.org/10.1016/j.abb.2024.110181
Received 15 June 2024; Received in revised form 9 October 2024; Accepted 10 October 2024
Available online 11 October 2024

commonly associated with glaucoma [22]. One of the key rationales for scrutinizing *h*CA II inhibitors was to explore their potential therapeutic benefits in treating glaucoma [23], which, if left untreated, can lead to blindness [24]. Furthermore, it is important to remember that *h*CA II, the physiologically dominant isoform of the *h*CAs family (as shown in Table 1), is widely expressed in a variety of brain cells and tissues, including but not limited to oligodendrocytes [25], astrocytes [26], myelin sheaths [27], choroid plexus [28], and myelinated tracts [29]. It is noteworthy that *h*CA II has been observed to be overexpressed in numerous tumor types [30], and such overexpression has often been linked to the heightened aggressiveness of tumor cells [31], as is evidenced, for instance, in the case of colorectal cancer and synchronous distant metastases [32].

Sulfonamides and their bioisosteres are widely acknowledged as significant pharmacophores exhibiting diverse biological activities, including *h*CA inhibition. Notably, sulfanilamide, discovered in 1940, was the first organic carbonic anhydrase inhibitor (*h*CAI) [33]. Subsequently, an extensive collection of sulfonamide-based *h*CAIs was synthesized, from which several agents, including acetazolamide (AAZ), methazolamide, ethoxzolamide, brinzolamide, and zonisamide, have been employed for the significant clinical management of *h*CA-related ailments (Fig. 1) [34].

The maintenance of a cell's regular physiological processes depends critically on the movement of anions through cellular membranes, as Poulsen et al. [35] noted. Numerous small-molecule anion transporters have been reported thus far, which are based on urea [36], thioureas [37], and sulfonamides [38]. As a result of their significant pharmacological properties, sulfonamide compounds derived from urea and theirs sulfur analogue thiourea have been continually employed in developing new bioactive compounds. Sulphamethazine (**SM**) is a sulfonamide that contains pyrimidine [39] with methyl substituents at the 4- and 6-positions and a *p*-aminobenzenesulfonamide group at the 2-position. It is an anti-infective agent [40], a carcinogenic agent [41], an antibacterial drug [42], an antimicrobial agent [43], a dihydropteroate synthase inhibitor [44], an environmental contaminant [45], a xenobiotic [46], and a drug allergen [47], and cholinesterases and α-glucosidase inhibitors (compound **2c**) [48] (Fig. 2).

Our design strategy is centered upon the preservation of the pharmacophoric moiety in sulphamethazine (i.e., 4-amino-*N*-(4,6-dimethylpyrimidin-2-yl)benzenesulfonamide) within our target molecules. We intend to augment this by introducing the amino functionality to triazene. By incorporating a variety of substituted phenyl tail moieties, it is anticipated that the catalytic zinc-ion of *h*CA will be bound, and that *h*CAs selectivity will be induced via different interactions with hydrophilic/hydrophobic amino acid residues in the ligand binding pocket (Fig. 3).

Table 1
A comprehensive overview of human carbonic anhydrases (*h*CAs) distribution across various organs or tissues and their subcellular localization.

*h*CAs	Organ or tissue distribution	Subcellular localization
I	Erythrocytes, eye, and gastrointestinal tract	Cytosol
II	Erythrocytes, eye, gastrointestinal tract, bone osteoclasts, brain, kidneys, lungs, and testes	Cytosol
III	Adipocytes and skeletal muscles,	Cytosol
IV	Eye, brain capillaries, kidneys, colon, heart muscle, lungs, and pancreas	Membrane-bound
VA	Brain and liver	Mitochondria
VB	Kidneys, gastrointestinal tract, heart or skeletal muscles, pancreas, and spinal cord	Mitochondria
VI	Salivary and mammary glands	Secreted
VII	Central nervous system	Cytosol
IX	Hypoxic tumors and gastrointestinal mucosa	Transmembrane
XII	Eye, hypoxic tumors, kidneys, and intestinal and reproductive epithelia	Transmembrane
XIII	Brain, kidneys, gut, lungs, and reproductive tract	Cytosol
XIV	Brain, liver, and kidneys	Transmembrane

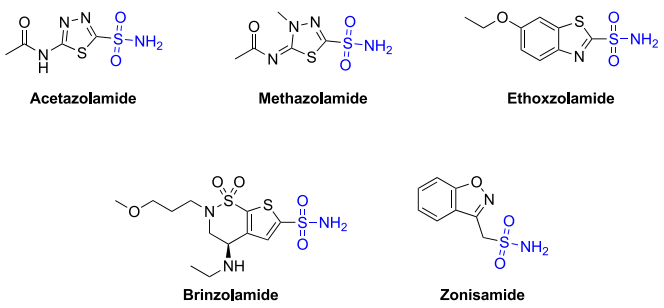

Fig. 1. Chemical compositions of certain commercially marketed *h*CA inhibitors based on sulfonamide.

Our research group is engaged in a perpetual endeavor to fabricate lead molecules that exhibit multi-targeting capabilities featuring isoform selective *h*CA inhibition, further enhanced by other interesting biological properties. We recently published our findings on synthesizing novel benzenesulfonamides demonstrating considerable isoform selective *h*CA inhibition [49–51]. Motivated by our earlier discoveries, we present a series of ten novel 1,3-diaryltriazene-substituted sulphamethazine derivatives **SM(1–10)** (depicted in Scheme 1) and their biological evaluation as inhibitors of *h*CA isoforms I and II.

2. Result and discussion

2.1. Drug design strategy and chemistry

The inspiration driving the design and synthesis of these new compounds **SM(1–10)** is derived from our most recent investigations [50,51]. IR spectroscopy and TLC tracked the target compounds' production reactions. The resulting-colored solid underwent filtering, many cold-water washings, and vacuum drying before being dried. By using FT-IR, ^{1}H and ^{13}C NMR, elemental analysis, and melting points, the obtained pure compounds **SM(1–10)** were thoroughly characterized. Both analytical and spectroscopic findings in the experimental part confirm the structure of the target compounds. These investigations highlighted the impressive and selective inhibition capabilities of newly synthesized derivatives containing 1,3-diaryltriazene-substituted sulphanilamide and metanilamide against the prominent isoform *h*CA II. With this knowledge as a foundation, our current endeavor sought to modify the sulfonamide group from primary to secondary amine. This modification was then applied to *h*CA I and II isozymes to assess how this alteration in the binding group might impact potency and selectivity. Our goal was to enhance the biological effectiveness of 1,3-diaryltriazene-substituted sulfonamides by altering the amine component from primary to secondary (specifically, from sulphanilamide to sulphamethazine) (Fig. 3). We aimed to investigate the potential efficacy of these compounds versus *h*CAs, namely, *h*CA I and II isoforms.

2.2. Carbonic anhydrase inhibitory effect of the target compounds SM (1–10)

The efficacy of the newly synthesized target 1,3-diaryltriazene-substituted sulfamethazine derivatives **SM(1–10)** was evaluated using Verpoorte's esterase assay technique [52]. Specifically, the ubiquitous cytosolic isoforms *h*CA I and II were tested for their capacity to inhibit using these substances. To determine the inhibition profile of the synthesized compounds for these *h*CA isoforms, as well as their selectivity profile, i.e., inhibition constants (K_I) and coefficients of determination (R^2), a comparison was made to the reference drug acetazolamide (AAZ) as indicated in Table 2 and Fig. 4.

All of the synthesized sulphamethazines **SM(1–10)** exhibited potent inhibition potency towards the physiologically significant cytosolic isoform *h*CA I with K_I constants ranging from 5.69 ± 0.59 nM to 77.08

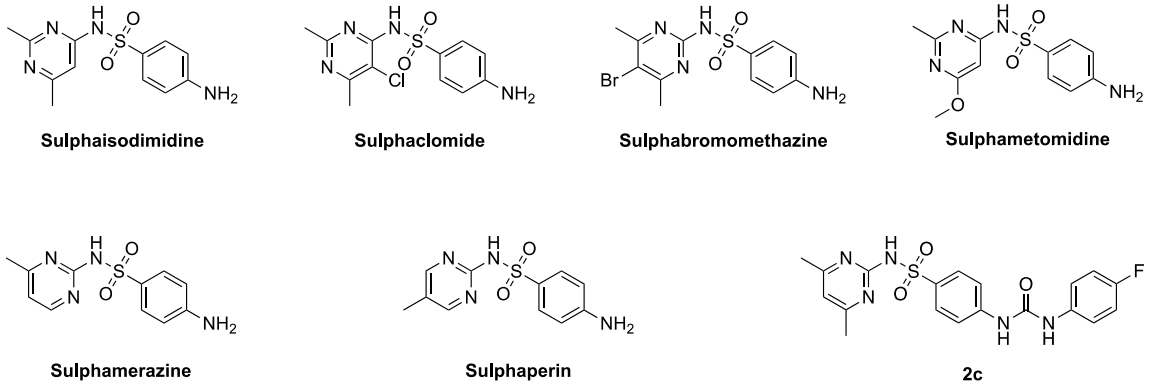

Fig. 2. Chemical compositions of various medications derived from pyrimidinyl sulfonamide that are sold commercially, as well as compound **2c**.

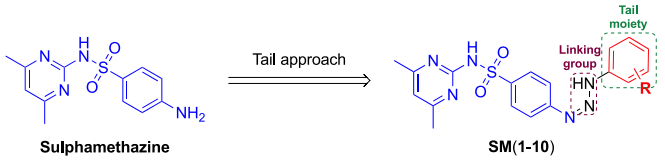

Fig. 3. Design of the novel synthesized 1,3-diaryltriazene-substituted sulphamethazines **SM**(**1**–**10**).

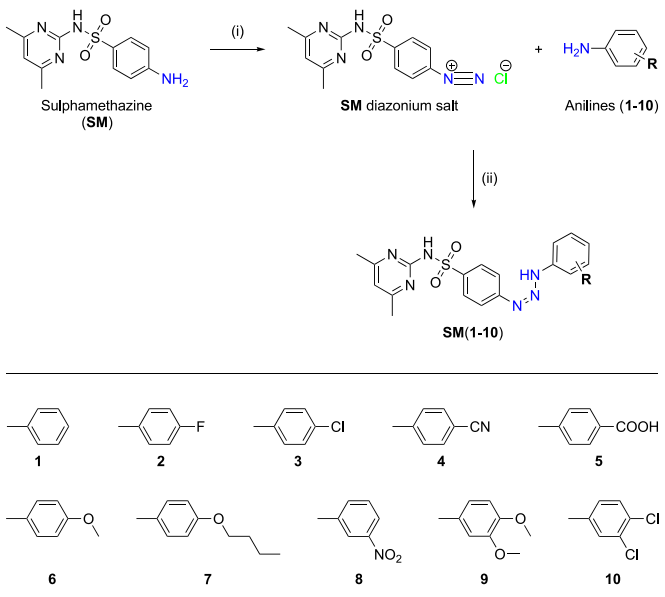

Scheme 1. The general synthetic route for synthesizing the novel sulphamethazines **SM**(**1**–**10**). (i) H_2O, HCl, and $NaNO_2$, 0–5 °C, 30 min, (ii) Substituted aromatic anilines (**1**–**10**), MeOH, H_2O, and sodium acetate, 0–5 °C 3 h, r. t. overnight.

± 5.09 nM in comparison to the standard drug, AAZ (K_I of 116.00 ± 8.48 nM). Compound **SM7** displayed the most potent inhibition of *h*CA I. Additionally, four compounds out of the ten novel sulphamethazines reported herein demonstrated more than four times more potent inhibition of the ubiquitous isoform *h*CA I than AAZ. In a more extensive sense, the compounds containing butoxy, chlorine, carboxyl, and cyano in R moiety **SM7** (K_I of 5.69 ± 0.59 nM), **SM3** (K_I of 11.33 ± 0.74 nM), **SM5** (K_I of 26.31 ± 2.05 nM), and **SM4** (K_I of 27.18 ± 3.08 nM), respectively, were discovered to be the strongest inhibitors. Interestingly, it was observed that the inhibitor with unsubstituted phenyl ring,

Table 2
Inhibition data of *h*CA isoforms I and II with novel synthesized 1,3-diaryltriazene-substituted sulphamethazine derivatives **SM**(**1**–**10**) compared to acetazolamide as reference inhibitor.

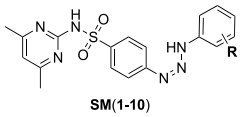

Compound		*h*CA I		*h*CA II		Selectivity index[b]	
ID	**R**	**K_I (nM)** [a]	**R^2**	**K_I (nM)** [a]	**R^2**	**I/II**	**II/I**
SM1	H	35.62 ± 4.12	0.9851	23.89 ± 2.38	0.9863	1.49	0.67
SM2	4-F	77.08 ± 5.09	0.9862	36.92 ± 4.03	0.9842	2.09	0.48
SM3	4-Cl	11.33 ± 0.74	0.9853	56.40 ± 5.08	0.9843	0.20	**4.98**
SM4	4-CN	27.18 ± 3.08	0.9846	**5.87 ± 0.57**	0.9867	4.63	0.22
SM5	4-COOH	26.31 ± 2.05	0.9855	15.49 ± 1.62	0.9851	1.70	0.59
SM6	4-OCH_3	37.69 ± 2.91	0.9845	7.07 ± 0.76	0.9842	5.33	0.19
SM7	4-OC_4H_9	**5.69 ± 0.59**	0.9858	12.87 ± 1.27	0.9875	0.44	2.26
SM8	3-NO_2	40.79 ± 4.68	0.9841	16.27 ± 1.72	0.9843	2.51	0.40
SM9	3,4-diOCH_3	74.98 ± 10.49	0.9851	7.54 ± 0.79	0.9844	**9.94**	0.10
SM10	3,4-diCl	69.03 ± 7.65	0.9857	14.63 ± 1.42	0.9866	4.72	0.21
AAZ [c]	–	116.00 ± 8.48	0.9850	57.25 ± 4.15	0.9858	–	–

[a] The test results were expressed as means of triplicate assays ± SEM.
[b] A high-value ratio characterizes a potent, selective inhibitor.
[c] Acetazolamide.

SM1 exhibited higher potency against *h*CA I compared to those with 4-fluorine, 4-methoxy, 4-nitro, 3,4-dimethoxy, and 3,4-dichlorine substitution on phenyl ring (**SM2**, **SM6**, and **SM8**-**10**) displayed the weakest inhibition in the respective series. This information is summarized in Table 2.

All of the sulphamethazine derivatives **SM**(**1**–**10**) that were tested demonstrated a promising inhibition profile against another cytosolic isoform *h*CA II associated with glaucoma with K_I values ranging from 5.87 ± 0.57 nM to 56.40 ± 5.08 nM. Specifically, ten compounds exhibited superior inhibition of isoform *h*CA II compared to the

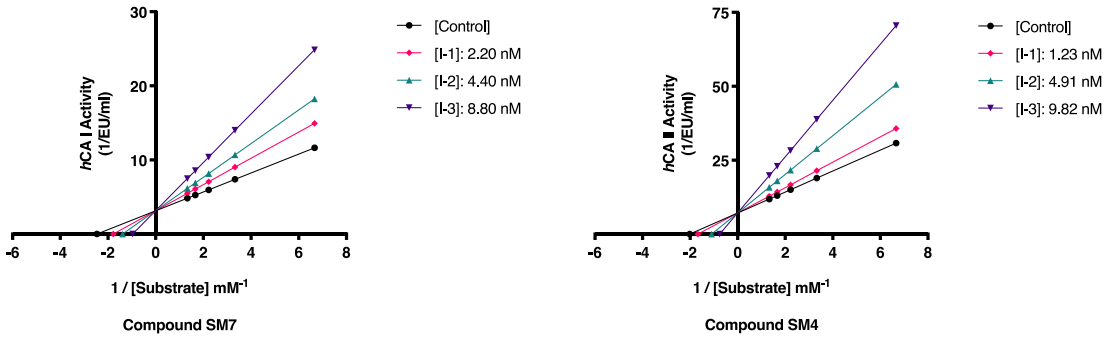

Fig. 4. *In vitro* effects of the novel synthesized 1,3-diaryltriazene-substituted sulphamethazines, 4-[3-(4-butoxyphenyl)triaz-1-en-1-yl]-*N*-(4,6-dimethylpyrimidin-2-yl)benzenesulfonamide (**SM7**) and 4-[3-(4-cyanophenyl)triaz-1-en-1-yl]-*N*-(4,6-dimethylpyrimidin-2-yl)benzenesulfonamide (**SM4**) against *h*CA I (left) and *h*CA II (right) activity, respectively. The K_I constants and kinds of inhibition for these substances were determined using Lineweaver-Burk plots. For this, three different inhibitor dosages for substances **SM7** and **SM4**, as well as five different 4-nitrophenyl acetate concentrations, were tested.

reference compound AAZ (K_I of 57.25 ± 4.15 nM). Notably, 4-cyano **SM4**, 4-methoxy **SM6**, and 3,4-dimethoxy **SM9** substituted compounds displayed sub-nanomolar inhibition, with K_I constants of 5.87 ± 0.57 nM, 7.07 ± 0.76 nM, and 7.54 ± 0.79 nM, respectively (refer to Table 2).

2.3. SAR parameters of the target compounds

The observed differences in the *h*CA I and II inhibitory activity of the 1,3-diaryl-substituted triazenes analogues **SM(1–10)** may be explained by the varied substituent patterns on the phenyl ring of the molecule, according to the study of the structure-activity relationship (SAR). All synthesized compounds **SM(1–10)** exhibited strong inhibition potential versus the cytosolic isoform *h*CA I compared to the standard drug AAZ. Among these compounds, compound **SM7** exhibited the strongest inhibition of *h*CA I. Compound **SM7** differs from other compounds in having a butoxy group at the fourth position of the phenyl ring. The butoxy group linked to the phenyl group interacted with the active Zn^{2+} metal center site of *h*CA I in the docking poses against it, which is an interesting finding. The chemicals studied here do not all possess a free sulfonamide group (-SO_2NH_2) [53] that binds directly to the Zn^{2+} of *h*CAs. However, all could still effectively inhibit this enzyme, which is intriguing. Molecular docking studies have shown that in addition to hydrogen bonding interaction with Tyr204 and forming specific favourable hydrophobic interactions, these molecules can inhibit the enzyme by fitting into the entrance of the active site such that the aryl group is displaced.

Similarly, all synthesized compounds **SM(1–10)** showed potent inhibitory potential against another cytosolic isoform *h*CA II compared to the reference drug AAZ. Among these compounds, compound **SM4** exhibited the most potent inhibition of *h*CA II. The difference between **SM4** from other compounds is the presence of a cyano group at the fourth position of the phenyl ring. In the *silico* study, in docking poses against *h*CA II, the cyano group attached to the phenyl group interacted with the active Zn^{2+} metal center region of *h*CA II [54]. In addition, the observation of two hydrogen bonds between the nitrogen atom of the Triazene group and Gln92 and between the nitrogen atom of the pyrimidine ring and the H_2O molecule and the formation of hydrophobic interactions with some amino acid residues contributed to the inhibition of the active site of this molecule.

2.4. In silico simulations

The *h*CAs' X-ray crystallographic structures (PDB IDs 1AZM and 3HS4 for *h*CA I and II, respectively) were used to examine the binding patterns of the novel synthesized 1,3-diaryltriazene-substituted sulphamethazines **SM(1–10)** and gain insight into the structural factors governing the enzyme-inhibitor complex. Initially, the enzyme binding sites were subjected to re-docking of the native ligand 5-acetamido-1,3,4-thiadiazole-2-sulfonamide (AZM or AAZ) to verify the soundness of the docking setup. The low RMSD values (0.34 and 1.20 Å, respectively) and capacity of the docking poses of the co-crystalized ligands to faithfully reproduce essential interactions demonstrated the viability of the employed docking approach (Fig. S1). The validated setup was used to investigate how these new sulphamethazines attach to the *h*CAs' active sites. Subsequently, the most potent inhibitors, **SM7** and **SM4**, respectively, and compound **SM9**, which has a selectivity index of 9.94, were docked into the binding sites of the *h*CAs (1AZM and 3HS4) crystallographic structures. The reported amino acids contributing to the isozymes *h*CA I and II inhibition were used to justify the qualitative binding poses.

Compound **SM7** displayed hydrophobic interactions with Trp 5, Tyr20, Phe 91, Ala 121, Leu 131, Leu 132, Ala 135, Leu141, Val143, Leu198, Pro 201, Pro202, Val 207, and Trp 209 residues and exhibited a docking score of approximately −3.767 kcal/mol. Furthermore, a network of hydrogen bonds with Tyr204 (at a distance of 1.81 Å) kept one of the oxygen atoms of its sulfonamide group in place. These docking positions for the inhibitor SM7 can explain why *h*CA I is inhibited (Fig. 5). With a docking score of −3.354 kcal/mol, the molecule **SM4**'s interaction with the active site residues revealed various interactions, including van der Waals forces, hydrogen bonds, and metal coordination. Between the nitrogen atom of the triazene group and Gln92, at a distance of 2.39 Å, and the nitrogen atom of the pyrimidine ring and the H_2O molecule, at a distance of 2.18 Å, two hydrogen bonds were seen. The nitrogen atom of the cyano group was also coordinated with the zinc-ion. Additionally, the amino acids Ile 91, Val 121, Phe 131, Leu141, Val143, Leu198, and Pro202 established hydrophobic contacts with compound **SM4**, which helped to keep **SM4** stable at the active site (Fig. 6).

The binding of compound **SM9** to the *h*CA II isoform exhibits notable selectivity, as indicated by the selectivity index of 9.94. This selectivity may be attributed to the interactions of **SM9** with Gln92 and a water molecule (distances of 2.36 Å and 2.19 Å) in the *h*CA II binding pocket. In contrast, in the *h*CA I binding pocket, **SM9** primarily interacts with Thr204 (distance of 2.10 Å) through hydrogen bonding. These specific interactions in the *h*CA II binding pocket may allow for a stronger binding of **SM9** to this isoform. It is worth noting that the hydrogen bonds and distances between **SM9** and *h*CA II are essential for the observed selectivity. In conclusion, these unique binding characteristics may enable **SM9** to fit more securely in the *h*CA II binding cavity (Fig. S2).

Additionally, the determination of physicochemical and

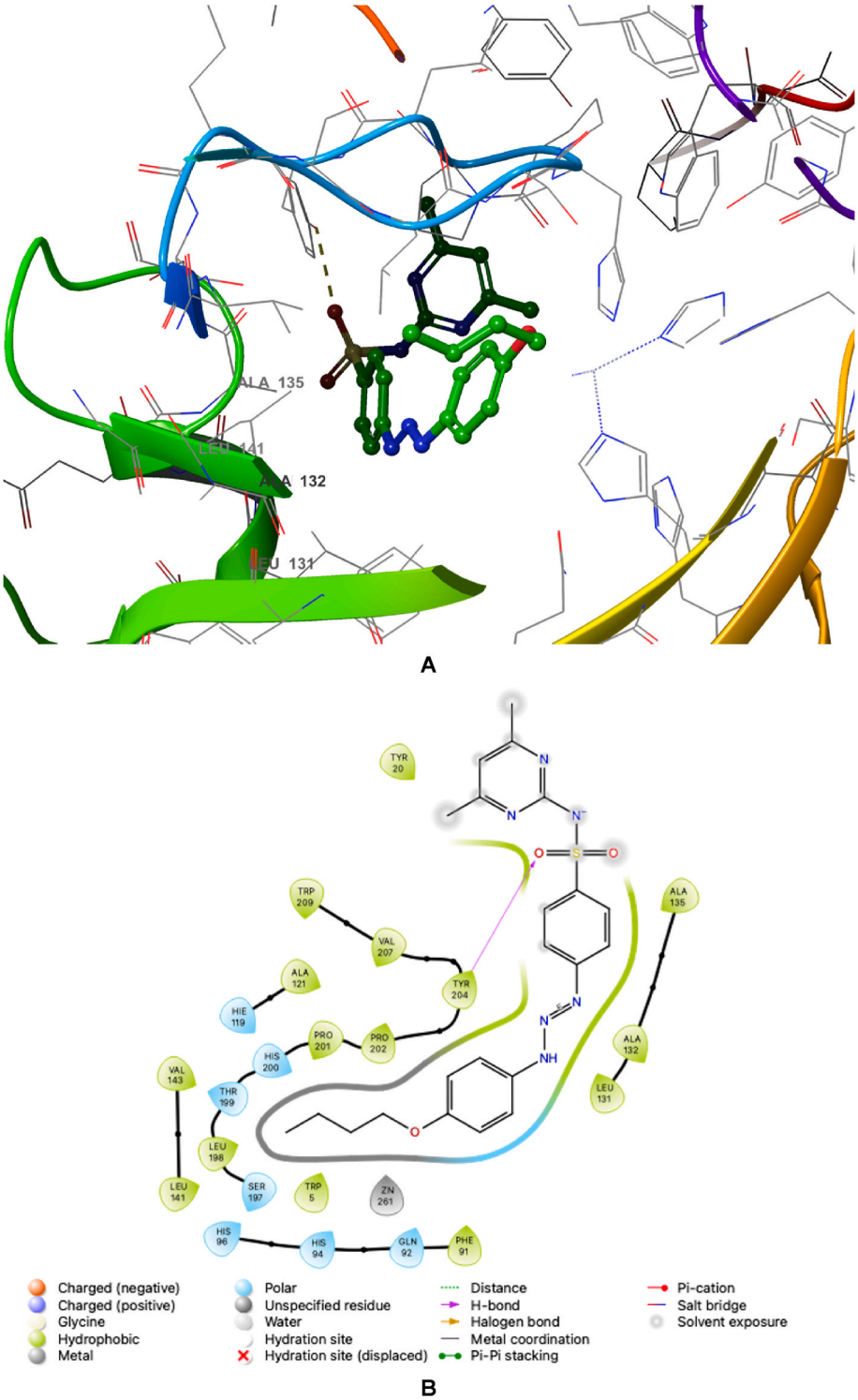

Fig. 5. Predicted binding mode of [3-(4-butoxyphenyl)triaz-1-en-1-yl]-*N*-(4,6-dimethylpyrimidin-2-yl)benzenesulfonamide (**SM7**) within *h*CA I isoform active site (PDB ID 1AZM). The figures include **A)** 3D and **B)** 2D images to further illustrate the interplay of amino acids.

pharmacokinetic properties of target compounds through *in silico* methods is an indispensable tool in the development of novel drug molecules. As such, a comprehensive assessment of drug-likeness in the synthesized agents was conducted through *in silico* physiochemical properties and ADME predictions for all compounds **SM(1–10)** using the QikProp module of Schrödinger Suite. The results of this analysis are presented in Table 3 and Fig. 7. The parameters of Lipinski's rule of five [55], which serve as a primary criterion for predicting drug-likeness and the potential for high oral absorption of a molecule, were calculated for all compounds. It is noteworthy that only **SM8** displayed a single violation of Lipinski's rule of five, which is deemed acceptable. This finding indicates that these compounds possess drug-like properties and have the potential to become orally active drugs.

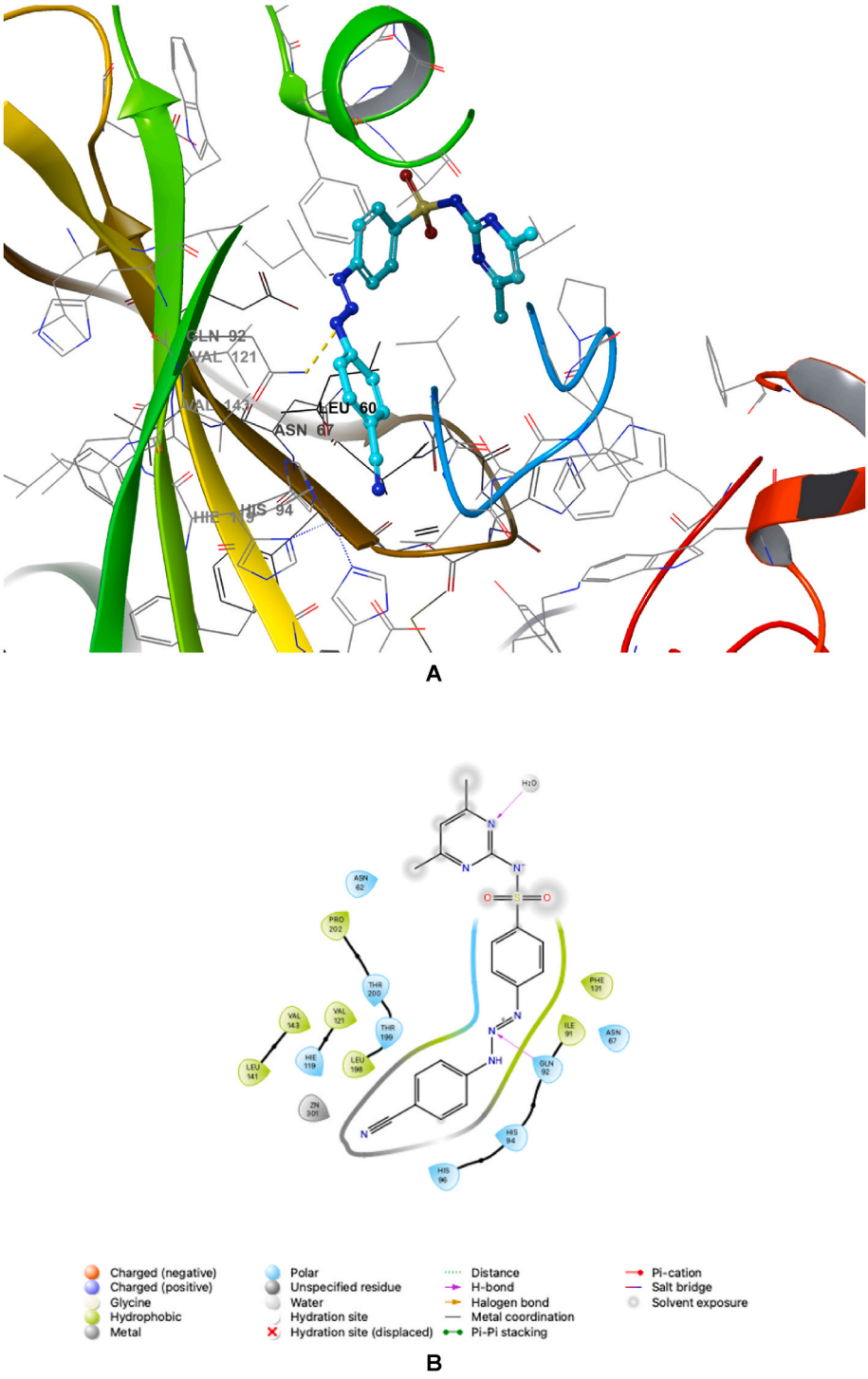

Fig. 6. Predicted binding mode of 4-[3-(4-cyanophenyl)triaz-1-en-1-yl]-*N*-(4,6-dimethylpyrimidin-2-yl)benzenesulfonamide (**SM4**) within *h*CA II isoform active site (PDB ID 3HS4). The figures include **A)** 3D and **B)** 2D images to further illustrate the interplay of amino acids.

3. Conclusion

Carbonic anhydrases play a pivotal role in catalyzing the reversible hydration of carbon dioxide to bicarbonate, as well as facilitating various hydrolytic processes. To date, seven distinct genetic families of *h*CAs have been identified, and extensive kinetic and X-ray crystallographic analyses have provided invaluable insights into the intricate structure-function relationships within this protein superfamily. Detailed elucidation of both activation and inhibition mechanisms has been achieved, with the recent discovery of numerous novel inhibitor classes further enhancing our understanding of the functional dynamics of *h*CAs, paving the way for future therapeutic innovations. In this study, in summary, we present a collection of ten new compounds, namely **SM (1–10)**, produced through the reaction between the diazonium salt of sulphamethazine and a range of aromatically substituted amines. This investigation centered on the synthesis and assessment of innovative derivatives featuring 1,3-diaryltriazene-substituted sulphamethazines **SM(1–10)** with the intent of inhibiting *h*CA I and II isozymes. The synthesized compounds on both isozymes showed significant inhibitory effects with competitive or non-competitive inhibition types at the

Table 3
ADME/Tox related parameters[a] of novel synthesized 1,3-diaryltriazene-substituted sulphamethazine derivatives **SM(1–10)** and the reference inhibitor acetazolamide.

Compounds ID	CNS	MW	Dipole	Volume	donorHB	acceptHB	QPlogPoct	QPlogPw	QPlogPo/w	QPlogS	QPlogHERG	QPPCaco	QPlogBB	QPlogKp	Metab	QPlogKhsa	HOA	PSA	Rule of Five
SM1	−2	382.4	6.7	1218.4	2.0	10.0	22.9	16.6	2.1	−4.8	−7.2	442	−1.4	−2.2	5	−0.3	86.7	108.0	0
SM2	−2	400.4	6.3	1236.8	2.0	10.0	23.1	16.3	2.4	−5.1	−7.0	443	−1.3	−2.3	4	−0.2	88.2	107.9	0
SM3	−2	416.9	6.3	1265.0	2.0	10.0	23.6	16.3	2.6	−5.4	−7.0	443	−1.2	−2.4	4	−0.2	89.6	107.9	0
SM4	−2	407.4	7.7	1285.9	2.0	11.5	24.7	18.1	1.4	−5.7	−7.1	92	−2.3	−3.5	4	−0.5	70.2	133.5	0
SM5	−2	426.4	7.5	1302.5	3.0	12.0	26.6	20.1	1.5	−4.7	−5.2	11	−2.7	−4.3	4	−0.6	54.2	157.4	0
SM6	−2	412.5	7.8	1272.7	2.0	10.8	23.7	16.6	2.0	−4.5	−6.6	350	−1.5	−2.6	5	−0.3	84.2	113.4	0
SM7	−2	454.5	8.0	1467.1	2.0	10.8	25.4	16.2	3.1	−5.9	−7.1	349	−1.9	−2.3	5	0.0	90.8	112.2	0
SM8	−2	427.4	9.6	1293.7	2.0	11.0	24.9	17.6	1.4	−4.9	−7.0	53	−2.6	−4.1	6	−0.3	53.1	152.8	1
SM9	−2	442.5	6.7	1371.7	2.0	11.5	24.7	17.0	2.3	−5.2	−6.9	442	−1.6	−2.4	6	−0.3	87.7	122.6	0
SM10	−2	451.3	7.1	1305.5	2.0	10.0	24.3	16.1	3.0	−6.0	−6.9	442	−1.1	−2.5	4	−0.1	92.1	107.9	0
AAZ[b]	−2	222.2	10.9	634.3	3.0	9.0	17.6	15.2	−1.8	−1.6	−3.8	36	−1.8	−5.9	1	−1.0	44.4	133.3	0

[a] CNS, Central nervous system activity (−2 inactive, +2 active); MW, molecular weight of the compound (130.00–725.00); Dipole, computed dipole moment of the compound (1.00–12.50); Volume, total solvent-accessible volume in cubic angstroms using a probe with a 1.4 Å Radius (500.00–2000.00); donorHB, estimated number of hydrogen bonds that would be donated by the solute to water molecules in an aqueous solution (0–6); acceptHB, estimated number of hydrogen bonds that would be accepted by the solute from water molecules in an aqueous solution (2–20); QPlogPoct, octanol/gas partition coefficient (8.00–35.00); QPlogPw, water/gas partition coefficient (4.00–45.00); QPlogPo/w, octanol/water partition coefficient (−2.00 - 6.50); QPlogS, aqueous solubility (−6.50 - 0.50); QPlogHERG, IC50 value for blockage of HERG K+ channels (concern below −5); QPPCaco, apparent Caco-2 cell permeability in nm/sec (<25 poor, great>500); QPlogBB, brain/blood partition coefficient (−3.00 - 1.20); QPlogKp, skin permeability (−8.00 to −1.00); Metab, number of likely metabolic reactions (1–8); QPlogKhsa, prediction of binding to human serum albumin (−1.50 - 1.50); HOA; human oral absorption (<25 % poor, high>80 %); PSA, van der Waals surface area of polar nitrogen and oxygen atoms (7.00–200.00); Rule of Five, number of violations of Lipinski's rule of five (max. 4).
[b] Acetazolamide.

nanomolar scale. Significantly, the newly devised derivatives displayed superior inhibitory potential compared to the reference drug AAZ versus *h*CAs. An analysis of the SAR elucidated that the arrangement of the R variable on the 1,3-diaryltriazene-substituted sulphamethazine derivatives significantly influenced the inhibitory activity on both *h*CA I and II. *In silico* simulations verified the binding affinity of the most effective inhibitors (**SM7** for *h*CA I and **SM4** for *h*CA II) by accurately simulating crucial interactions in the target enzymes' active regions. The observed differences in affinity and selectivity across the derivatives were attributable to various structural changes that produced distinctive steric and binding properties. Overall, the newly synthesized sulphamethazine compounds show promise as effective *h*CA inhibitors, highlighting their potential for further development in the field of enzyme inhibition. Future research should focus on designing and developing alternative agents with the potential to effectively treat or prevent ailments linked to glaucoma and *h*CA inhibition.

4. Experimental

4.1. General synthesis method for the preparation of novel sulphamethazines SM(1–10)

According to our prior research, the compounds **SM(1–10)** were created using our improved reaction conditions. In summary, after cooling a mixture of sulphamethazine (5 mmol) in 2 ml of concentrated hydrochloric acid and 15 ml of water to 0–5 °C, sodium nitrite (7 mmol) in 5 ml of water was slowly added while stirring continuously for 15–20 min. The mixture was agitated for 30 min at 0–5 °C before diazonium solution was added to the aniline solution, which had been made by dissolving 5 mmol of substituted anilines in 5 ml of MeOH and correcting the pH to 6–7 at the same time. The reaction mixture was then agitated for 3 h at 0–5 °C and overnight at room temperature in the dark (Scheme 1). With the help of TLC and IR spectroscopy, reactions were tracked. The colorful solid was filtered out, repeatedly washed in cold water, crystallized using the proper solvents, and dried under a vacuum. Spectroscopic and analytical techniques were used to characterize the obtained pure compounds **SM(1–10)** in detail (FT-IR, ^{1}H and ^{13}C NMR, and melting points).

4.1.1. N-(4,6-dimethylpyrimidin-2-yl)-4-(3-phenyltriaz-1-en-1-yl) benzenesulfonamide (SM1)

Yield: 73 %; Color: orange solid; Melting Point: 187–189 °C; Anal. Calcd for $C_{18}H_{18}N_6O_2S$ (382.44 g/mol) (%): C, 56.53; H, 4.74; N, 21.98; S, 8.38, Found (%): C, 56.45; H, 4.79; N, 21.99; S, 8.35. FT-IR (cm^{-1}): 3238, 3212 (NH), 1592, 1381, 1144 (symmetric) (S═O), 1094; ^{1}H NMR (DMSO-d_6, 400 MHz, δ ppm): 12.54 (br.s, 2H, –NH–), 7.96 (d, J = 8.4 Hz, 2H, Ar–H), 7.53-7.41 (m, 6H, Ar–H), 7.25 (t, 1H, Ar–H), 6.67 (s, 1H, Ar–H (pyrimidine)), 3.41 (s, 6H, –CH_3); ^{13}C NMR (DMSO-d_6, 100 MHz, δ ppm): 172.67, 170.77, 157.90, 147.31, 136.17, 130.28, 129.77, 126.82, 119.74, 115.30, 113.36, 23.43.

4.1.2. N-(4,6-dimethylpyrimidin-2-yl)-4-[3-(4-fluorophenyl)triaz-1-en-1-yl]benzenesulfonamide (SM2)

Yield: 89 %; Color: yellow solid; Melting Point: 213–215 °C; Anal.

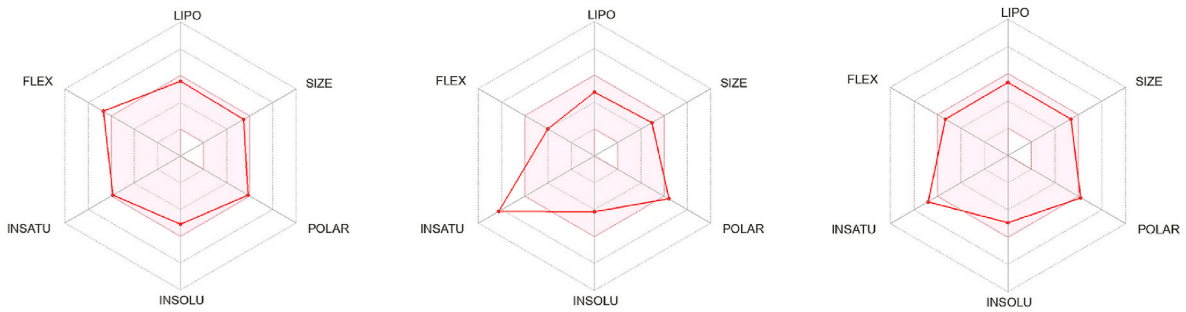

Fig. 7. Diagrams showing 'drug-likeness' descriptors for the most potent inhibitors 4-[3-(4-butoxyphenyl)triaz-1-en-1-yl]-*N*-(4,6-dimethylpyrimidin-2-yl)benzenesulfonamide (**SM7** against *h*CA I, left), 4-[3-(4-cyanophenyl)triaz-1-en-1-yl]-*N*-(4,6-dimethylpyrimidin-2-yl)benzenesulfonamide (**SM4** against *h*CA II, middle), and selective inhibitor 4-[3-(3,4-dimethoxyphenyl)triaz-1-en-1-yl]-*N*-(4,6-dimethylpyrimidin-2-yl)benzenesulfonamide (**SM9** against *h*CA I, right). The red-colored zone has been identified as a feasible physicochemical domain to enhance oral bioavailability. FLEX, flexibility; INSATU, saturation; INSOLU, insolubility; LIPO, lipophilicity; POLAR, polarity; SIZE, molecular weight.

Calcd for $C_{18}H_{17}FN_6O_2S$ (400.43 g/mol) (%): C, 53.99; H, 4.28; N, 20.99; S, 8.01, Found (%): C, 53.93; H, 4.30; N, 21.05; S, 7.96. FT-IR (cm^{-1}): 3248, 3220 (NH), 1594, 1345, 1151 (symmetric) (S═O), 1093; ^{1}H NMR (DMSO-d_6, 400 MHz, δ ppm): 12.79 (s, 1H, –NH–), 11.55 (br.s, 1H, –NH–), 7.97 (d, J = 8.4 Hz, 2H, Ar–H), 7.59-7.45 (m, 4H, Ar–H), 7.28 (t, 2H, Ar–H), 6.76 (s, 1H, Ar–H (pyrimidine)), 3.36 (s, 6H, $–CH_3$); ^{13}C NMR (DMSO-d_6, 100 MHz, δ ppm): 172.09, 167.84, 145.83, 134.28, 130.46, 122.97, 116.65, 116.43, 113.99, 23.39.

4.1.3. 4-[3-(4-Chlorophenyl)triaz-1-en-1-yl]-N-(4,6-dimethylpyrimidin-2-yl)benzenesulfonamide (SM3)

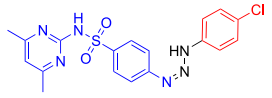

Yield: 92 %; Color: cream solid; Melting Point: 215–216 °C; Anal. Calcd for $C_{18}H_{17}ClN_6O_2S$ (416.88 g/mol) (%): C, 51.86; H, 4.11; N, 20.16; S, 7.69, Found (%): C, 51.83; H, 4.08; N, 20.19; S, 7.65.FT-IR (cm^{-1}): 3248, 3215 (NH), 1597, 1380, 1149 (symmetric) (S═O), 1088; ^{1}H NMR (DMSO-d_6, 400 MHz, δ ppm): 12.88 (s, 1H, –NH–), 11.63 (br.s, 1H, –NH–), 7.98 (d, J = 8.4 Hz, 2H, Ar–H), 7.55-7.41 (m, 6H, Ar–H), 6.76 (s, 1H, Ar–H (pyrimidine)), 3.35 (s, 6H, $–CH_3$); ^{13}C NMR (DMSO-d_6, 100 MHz, δ ppm): 167.79, 156.79, 130.39, 129.75, 128.94, 122.32, 115.70, 114.02, 23.38.

4.1.4. 4-[3-(4-Cyanophenyl)triaz-1-en-1-yl]-N-(4,6-dimethylpyrimidin-2-yl)benzenesulfonamide (SM4)

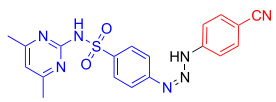

Yield: 85 %; Color: dark orange solid; Melting Point: 140–142 °C; Anal. Calcd for $C_{19}H_{17}N_7O_2S$ (407.45 g/mol) (%): C, 56.01; H, 4.21; N, 24.06; S, 7.87, Found (%): C, 55.97; H, 4.23; N, 24.11; S, 7.82. FT-IR (cm^{-1}): 3353, 3215 (NH), 2221 (CN), 1596, 1349, 1150 (symmetric) (S═O), 1078; ^{1}H NMR (DMSO-d_6, 400 MHz, δ ppm): 13.08 (br.s, 1H, –NH–), 11.72 (br.s, 1H, –NH–), 8.02 (d, J = 8.8 Hz, 2H, Ar–H), 7.85 (d, J = 8.8 Hz, 2H, Ar–H), 7.63-7.58 (m, 4H, Ar–H), 6.73 (s, 1H, Ar–H (pyrimidine)), 3.35 (s, 6H, $–CH_3$); ^{13}C NMR (DMSO-d_6, 100 MHz, δ ppm): 167.77, 157.03, 153.47, 134.24, 133.89, 130.08, 128.78, 119.54, 113.92, 95.98, 23.32.

4.1.5. 4-(3-{4-[N-(4,6-Dimethylpyrimidin-2-yl)sulfamoyl]phenyl}triaz-2-en-1-yl)benzoic acid (SM5)

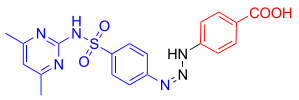

Yield: 89 %; Color: yellow solid; Melting Point: 226–227 °C; Anal. Calcd for $C_{19}H_{18}N_6O_4S$ (426.45 g/mol) (%): C, 53.51; H, 4.25; N, 19.71; S, 7.52, Found (%): C, 53.48; H, 4.27; N, 19.74; S, 7.48. FT-IR (cm^{-1}): 3326 (br.s NH and OH), 1684 (C═O), 1596, 1314, 1150 (symmetric) (S═O), 1085; ^{1}H NMR (DMSO-d_6, 400 MHz, δ ppm): 12.61 (br.s, 3H, 2x–NH–, and –OH), 8.03-7.97 (m, 4H, Ar–H), 7.62-7.54 (m, 4H, Ar–H), 6.76 (s, 1H, Ar–H (pyrimidine)), 3.37 (s, 6H, $–CH_3$); ^{13}C NMR (DMSO-d_6, 100 MHz, δ ppm): 167.99, 167.45, 156.67, 153.61, 131.70, 131.34, 130.22, 117.36, 113.86, 113.03, 23.32.

4.1.6. N-(4,6-dimethylpyrimidin-2-yl)-4-[3-(4-methoxyphenyl)triaz-1-en-1-yl]benzenesulfonamide (SM6)

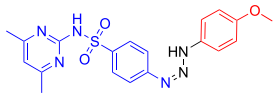

Yield: 92 %; Color: dark pink solid; Melting Point: 176–178 °C; Anal. Calcd for $C_{19}H_{20}N_6O_3S$ (412.47 g/mol) (%): C, 55.33; H, 4.89; N, 20.38; S, 7.77, Found (%): C, 55.29; H, 4.91; N, 20.41; S, 7.75. FT-IR (cm^{-1}): 3252, 3215 (NH), 1592, 1342, 1142 (symmetric) (S═O), 1089; ^{1}H NMR (DMSO-d_6, 400 MHz, δ ppm): 12.47 (s, 1H, –NH–), 11.55 (br.s, 1H, –NH–), 7.95 (d, J = 8.8 Hz, 2H, Ar–H), 7.52 (d, J = 8.4 Hz, 2H, Ar–H), 7.40 (d, J = 8.4 Hz, 2H, Ar–H), 7.10 (d, J = 8.8 Hz, 2H, Ar–H), 6.75 (s, 1H, Ar–H (pyrimidine)), 3.80 (s, 3H, $–OCH_3$), 3.31 (s, 6H, $–CH_3$), 2.57 (s, 3H, $–CH_3$); ^{13}C NMR (DMSO-d_6, 100 MHz, δ ppm): 167.79, 159.25, 157.01, 146.25, 133.63, 130.50, 122.49, 114.96, 113.92, 113.53, 55.83, 23.43.

4.1.7. 4-[3-(4-Butoxyphenyl)triaz-1-en-1-yl]-N-(4,6-dimethylpyrimidin-2-yl)benzenesulfonamide (SM7)

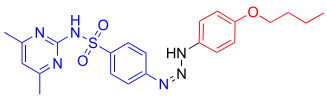

Yield: 78 %; Color: pink solid; Melting Point: 166–168 °C; Anal. Calcd for $C_{22}H_{26}N_6O_3S$ (454.55 g/mol) (%): C, 58.13; H, 5.77; N, 18.49; S, 7.05, Found (%): C, 58.10; H, 5.79; N, 18.53; S, 7.01. FT-IR (cm^{-1}): 3240, 3216 (NH), 1591, 1349, 1150 (symmetric) (S═O), 1093; ^{1}H NMR (DMSO-d_6, 400 MHz, δ ppm): 12.50 (br.s, 1H, –NH–), 11.52 (br.s, 1H,

–NH–), 7.94 (d, J = 8.0 Hz, 2H, Ar–H), 7.50 (d, J = 8.4 Hz, 2H, Ar–H), 7.39 (d, J = 8.4 Hz, 2H, Ar–H), 6.99 (d, J = 8.0 Hz, 2H, Ar–H), 6.72 (s, 1H, Ar–H (pyrimidine)), 3.99 (t, 2H, -O$\underline{CH_2}CH_2CH_2CH_3$), 3.37 (s, 6H, –$CH_3$), 1.73-1.65 (m, 2H, -OCH$_2\underline{CH_2}CH_2CH_3$) 1.46-1.140 (m, 2H, –OCH$_2$CH$_2\underline{CH_2}CH_3$), 0.93 (t, 3H, –OCH$_2$CH$_2$CH$_2\underline{CH_3}$); ^{13}C NMR (DMSO-d_6, 100 MHz, δ ppm): 167.74, 158.71, 157.12, 142.72, 130.78, 122.41, 115.53, 113.84, 113.48, 67.86, 31.28, 23.43, 19.19, 14.34.

4.1.8. N-(4,6-dimethylpyrimidin-2-yl)-4-[3-(3-nitrophenyl)triaz-1-en-1-yl]benzenesulfonamide (SM8)

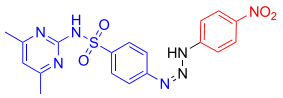

Yield: 74 %; Color: light brown solid; Melting Point: 209–210 °C; Anal. Calcd for $C_{18}H_{17}N_7O_4S$ (427.44 g/mol) (%): C, 50.58; H, 4.01; N, 22.94; S, 7.50, Found (%): C, 50.54; H, 4.07; N, 22.98; S, 7.45. FT-IR (cm^{-1}): 3264, 3211 (NH), 1597, 1348, 1153 (symmetric) (S═O), 1079; ^{1}H NMR (DMSO-d_6, 400 MHz, δ ppm): 13.13 (br.s, 1H, –NH–), 11.80 (br.s, 1H, –NH–), 8.20 (s, 1H, Ar–H), 8.08-8.00 (m, 3H, Ar–H), 7.95 (d, J = 8.0 Hz, 1H, Ar–H), 7.71 (t, 1H, Ar–H), 7.56 (d, J = 8.4 Hz, 2H, Ar–H), 6.74 (s, 1H, Ar–H (pyrimidine)), 3.35 (s, 6H, –CH_3); ^{13}C NMR (DMSO-d_6, 100 MHz, δ ppm): 167.49, 157.02, 150.59, 149.35, 131.33, 130.79, 120.41, 113.66, 110.20, 107.46, 23.37.

4.1.9. 4-[3-(3,4-Dimethoxyphenyl)triaz-1-en-1-yl]-N-(4,6-dimethylpyrimidin-2-yl)benzenesulfonamide (SM9)

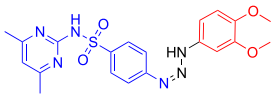

Yield: 94 %; Color: dark purplish red solid; Melting Point: 144–146 °C; Anal. Calcd for $C_{20}H_{22}N_6O_4S$ (442.49 g/mol) (%): C, 54.29; H, 5.01; N, 18.99; S, 7.25, Found (%): C, 54.25; H, 5.07; N, 19.04; S, 7.22. FT-IR (cm^{-1}): 3251, 3162 (NH), 1596, 1371, 1129 (symmetric) (S═O), 1081; ^{1}H NMR (DMSO-d_6, 400 MHz, δ ppm): 11.69 (br.s, 2H, –NH–), 8.05 (d, J = 8.4 Hz, 2H, Ar–H), 7.93 (d, J = 8.4 Hz, 2H, Ar–H), 7.14 (s, 1H, Ar–H), 6.99 (s, 1H, Ar–H), 6.76 (s, 1H, Ar–H (pyrimidine)), 6.43 (s, 1H, Ar–H), 3.81 (s, 3H, –OCH_3), 3.71 (s, 3H, –OCH_3), 3.36 (s, 6H, –CH_3); ^{13}C NMR (DMSO-d_6, 100 MHz, δ ppm): 167.78, 156.66, 155.08, 145.15, 142.09, 140.00, 130.01, 129.62, 121.61, 113.71, 98.55, 55.99, 23.24.

4.1.10. 4-[3-(3,4-Dichlorophenyl)triaz-1-en-1-yl]-N-(4,6-dimethylpyrimidin-2-yl)benzenesulfonamide (SM10)

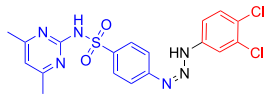

Yield: 89 %; Color: light brown solid; Melting Point: 196–197 °C; Anal. Calcd for $C_{18}H_{16}Cl_2N_6O_2S$ (451.33 g/mol) (%): C, 47.90; H, 3.57; N, 18.62; S, 7.10, Found (%): C, 47.86; H, 3.58; N, 18.66; S, 7.07. FT-IR (cm^{-1}): 3284, 3224 (NH), 1594, 1380, 1117 (symmetric) (S═O), 1073; ^{1}H NMR (DMSO-d_6, 400 MHz, δ ppm): 12.97 (br.s, 1H, –NH–), 11.68 (br. s, 1H, –NH–), 7.99 (d, J = 8.8 Hz, 2H, Ar–H), 7.73 (s, 1H, Ar–H), 7.66 (d, J = 8.8 Hz, 1H, Ar–H), 7.55-7.47 (m, 3H, Ar–H), 6.75 (s, 1H, Ar–H (pyrimidine)), 3.37 (s, 6H, –CH_3); ^{13}C NMR (DMSO-d_6, 100 MHz, δ ppm): 167.79, 156.75, 147.25, 135.94, 131.57, 130.87, 130.33, 120.55, 115.70, 113.67, 23.33.

4.2. Carbonic anhydrase inhibitory effect study

At a concentration of 3 mM, *p*-nitrophenyl acetate (PubChem CID: 13243) was employed as the substrate. The experiment was conducted at an absorbance of 348 nm. The buffer for assessing the catalytic activity of *h*CA isozymes I and II was 50 mM tris(hydroxymethyl)aminomethane/SO_4 pH 7.4. The *h*CA-catalysed esterase reaction's initial rate was monitored for 1–180 s according to Verpoorte's method [52]. Dissolution of 1,3-diaryltriazene-substituted sulphamethazine derivatives **SM(1–10)** and reference drug AAZ was carried out in DMSO at a starting concentration of 1 mg/ml. Subsequently, dilutions were made with the assay buffer. DMSO was found to be present in the final reaction mixture at a concentration of about 1 %. Before the experiment, inhibitor and enzyme solutions were pre-incubated together for 3 min at room temperature to allow for the development of the E-I complex. Each specimen underwent a triad of measurements. To scrutinize the *in vitro* inhibitory mechanisms of target compounds **SM(1–10)**, kinetic assays featuring an assortment of substrate and chemical concentrations were executed. The resultant data was subsequently utilized to construct Michaelis-Menten curves [56] and Lineweaver-Burk plots, while computing K_I values and pinpointing the inhibition types [57,58].

4.3. In silico study

Molecular docking analyses were conducted to examine the novel synthesized 1,3-diaryltriazene-substituted sulphamethazines **SM(1–10)** against *h*CAs. The Small-Molecule Drug Discovery Suite 2023-2 for Mac (Schrödinger, LLC, NY, USA) was employed for this purpose according to our previous study [59,60]. The protein crystal structures, PDB IDs 1AZM [61] and 3HS4 [62] for *h*CA isoforms I and II, respectively, were obtained from the RCSB protein data bank. These structures underwent processing with Schrödinger's Protein Preparation Workflow protocol [63], followed by default settings that check and correct issues such as missing hydrogen atoms, ionic states, bond order assignments, etc. Waters beyond 5 Å of het groups or with fewer than three hydrogen bonds to non-waters were removed. Restrained energy minimization was applied using the optimized potentials for liquid simulations-4 (OPLS4) force field. Ramachandran plots further checked prepared protein systems, ensuring there were no steric clashes. AAZ was selected as the grid-defining ligand for both the 1AZM and 3HS4 systems to generate receptor grids. Default van der Waals radius scaling parameters were used (partial charge cutoff of 0.25, scaling factor of 1). Grid box size was set as 10 × 10 × 10 Å with a spacing of 0.375 Å [64]. The ChemDraw program V21 for Mac (PerkinElmer, Inc., Waltham, MA, USA) was utilized to sketch the structures of the targeted sulphamethazines **SM(1–10)**. The LigPrep tool [65] in the OPLS force field was employed to prepare the 3D structures of the **SM(1–10)** according to default options. Epik was used to determine the appropriate ionization states at pH 7.4 [66]. The receptor grids were established by centering on the co-crystallized ligands, AZM (AAZ), within the protein structures using the Receptor Grid Generation module. Additionally, SiteMap software confirmed the validity of the *h*CAs binding site by determining the best score for the target ligand, AZM [67]. The Glide Ligand Docking panel executed the initial docking simulation utilizing the Standard Precision (SP) mode [68]. After completing the docking simulation, each docked conformation underwent post-docking minimization [69]. Additionally, the pharmacokinetic and ADME properties of the target **SM(1–10)** derivatives were determined using LigPrep-prepared 3D structures by QikProp tool [70].

4.4. Statistical study

The present study employed GraphPad Prism version 8 software for Mac, created by GraphPad Software (La Jolla, California, USA), to analyze data and generate graphs for the inhibitory effect study. The additional sum-of-squares F test and the AICc approach were employed

to compare the goodness of fit for the enzyme inhibition models. The findings were presented in the mean ± standard error of the mean format, alongside 95 % confidence intervals. Statistical significance was deemed present when the *p*-value was below 0.05.

CRediT authorship contribution statement

Nabih Lolak: Validation, Investigation, Formal analysis. **Cüneyt Türkeş:** Writing – original draft, Validation, Methodology, Investigation, Formal analysis, Conceptualization. **Suleyman Akocak:** Writing – original draft, Validation, Methodology, Investigation, Formal analysis, Conceptualization. **Hatice Esra Duran:** Validation, Investigation, Formal analysis. **Mesut Işık:** Methodology, Conceptualization. **Mustafa Durgun:** Methodology, Conceptualization. **Şükrü Beydemir:** Methodology, Funding acquisition, Conceptualization.

Data availability

Data is provided within the manuscript or supplementary information files.

Declaration of competing interest

The authors declare no competing interests.

Acknowledgement

This work was supported by the Research Fund of Anadolu University (grant number 2102S003).

Appendix A. Supplementary data

Supplementary data to this article can be found online at https://doi.org/10.1016/j.abb.2024.110181.

References

[1] C.T. Supuran, Carbonic anhydrase inhibitors: an editorial, Expert Opin. Ther. Pat. 23 (6) (2013) 677–679, https://doi.org/10.1517/13543776.2013.778246.
[2] A. Aspatwar, M.E.E. Tolvanen, S. Parkkila, Phylogeny and expression of carbonic anhydrase-related proteins, BMC Mol. Biol. 11 (1) (2010) 25, https://doi.org/10.1186/1471-2199-11-25.
[3] S. Kumar, S. Rulhania, S. Jaswal, V. Monga, Recent advances in the medicinal chemistry of carbonic anhydrase inhibitors, Eur. J. Med. Chem. 209 (2021) 112923, https://doi.org/10.1016/j.ejmech.2020.112923.
[4] Z. Alim, 1H-indazole molecules reduced the activity of human erythrocytes carbonic anhydrase I and II isoenzymes, J. Biochem. Mol. Toxicol. 32 (9) (2018) e22194, https://doi.org/10.1002/jbt.22194.
[5] E. Bayram, M. Senturk, O.I. Kufrevioglu, C.T. Supuran, In vitro inhibition of salicylic acid derivatives on human cytosolic carbonic anhydrase isozymes I and II, Bioorg. Med. Chem. 16 (20) (2008) 9101–9105, https://doi.org/10.1016/j.bmc.2008.09.028.
[6] P. Taslimi, C. Caglayan, İ. Gulcin, The impact of some natural phenolic compounds on carbonic anhydrase, acetylcholinesterase, butyrylcholinesterase, and α-glycosidase enzymes: an antidiabetic, anticholinergic, and antiepileptic study, J. Biochem. Mol. Toxicol. 31 (12) (2017) e21995, https://doi.org/10.1002/jbt.21995.
[7] F. Topal, Inhibition profiles of Voriconazole against acetylcholinesterase, α-glycosidase, and human carbonic anhydrase I and II isoenzymes, J. Biochem. Mol. Toxicol. 33 (10) (2019) e2238510, https://doi.org/10.1002/jbt.22385.
[8] Z. Alım, N. Kılınç, M.M. İşgör, B. Şengül, Ş. Beydemir, Some anti-inflammatory agents inhibit esterase activities of human carbonic anhydrase isoforms I and II: an in vitro study, Chem. Biol. Drug Des. 86 (4) (2015) 857–863, https://doi.org/10.1111/cbdd.12561.
[9] J.-Y. Winum, D. Vullo, A. Casini, J.-L. Montero, A. Scozzafava, C.T. Supuran, Carbonic anhydrase inhibitors. Inhibition of cytosolic isozymes I and II and transmembrane, tumor-associated isozyme IX with sulfamates including EMATE also acting as steroid sulfatase inhibitors, J. Med. Chem. 46 (11) (2003) 2197–2204, https://doi.org/10.1021/jm021124k.
[10] V. Alterio, A. Di Fiore, K. D'Ambrosio, C.T. Supuran, G. De Simone, Multiple binding modes of inhibitors to carbonic anhydrases: how to design specific drugs targeting 15 different isoforms? Chem. Rev. 112 (8) (2012) 4421–4468, https://doi.org/10.1021/cr200176r.
[11] H.E. Bostancı, U.A. Çevik, R. Kapavarapu, Y.C. Güldiken, Z.D.Ş. Inan, Ö.Ö. Güler, T.K. Uysal, A. Uytun, F.N. Çetin, Y. Özkay, Z.A. Kaplancıklı, Synthesis, biological evaluation and in silico studies of novel thiadiazole-hydrazone derivatives for carbonic anhydrase inhibitory and anticancer activities, SAR QSAR Environ. Res. 34 (7) (2023) 543–567, https://doi.org/10.1080/1062936X.2023.2240698.
[12] M. Abdoli, A. Bonardi, C.T. Supuran, R. Žalubovskis, Investigation of novel alkyl/benzyl (4-sulphamoylphenyl)carbamimidothioates as carbonic anhydrase inhibitors, J. Enzyme Inhib. Med. Chem. 38 (1) (2023) 2152811, https://doi.org/10.1080/14756366.2022.2152811.
[13] T. Tekeli, S. Akocak, A. Petreni, N. Lolak, S. Çete, C.T. Supuran, Potent carbonic anhydrase I, II, IX and XII inhibition activity of novel primary benzenesulfonamides incorporating bis-ureido moieties, J. Enzyme Inhib. Med. Chem. 38 (1) (2023) 2185762, https://doi.org/10.1080/14756366.2023.2185762.
[14] Y. Gök, P. Taslimi, B. Şen, S. Bal, A. Aktaş, M. Aygün, M. Sadeghi, İ. Gülçin, Design, synthesis, characterization, crystal structure, in silico studies, and inhibitory properties of the PEPPSI type Pd(II)NHC complexes bearing chloro/fluorobenzyl group, Bioorg. Chem. 135 (2023) 106513, https://doi.org/10.1016/j.bioorg.2023.106513.
[15] H. Yakan, G. Bilir, Ş. Çakmak, Ö. Taş, N. Türköz Karakullukçu, E. Soydan, H. Kütük, C. Güçlü, M. Şentürk, T. Arslan, S. Öztürk, E. Aksakal, D. Ekinci, Inhibitory effects of sulfenimides on human and bovine carbonic anhydrase enzymes, J. Enzyme Inhib. Med. Chem. 38 (1) (2023) 2194573, https://doi.org/10.1080/14756366.2023.2194573.
[16] R. Çakmak, E. Başaran, K. Sahin, M. Şentürk, S. Durdağı, Synthesis of Novel Hydrazide–Hydrazone Compounds and *In Vitro* and *In Silico*Investigation of Their Biological Activities against AChE, BChE, and hCA I and II, ACS Omega 9 (18) (2024) 20030–20041, https://doi.org/10.1021/acsomega.3c10182.
[17] D.M. Elimam, W.M. Eldehna, R. Salem, A. Bonardi, A. Nocentini, S.T. Al-Rashood, M.M. Elaasser, P. Gratteri, C.T. Supuran, H.A. Allam, Natural inspired ligustrazine-based SLC-0111 analogues as novel carbonic anhydrase inhibitors, Eur. J. Med. Chem. 228 (2022) 114008, https://doi.org/10.1016/j.ejmech.2021.114008.
[18] H. Singh, S.K. Vasa, H. Jangra, P. Rovó, C. Päslack, C.K. Das, H. Zipse, L.V. Schäfer, R. Linser, Fast microsecond dynamics of the protein–water network in the active site of human carbonic anhydrase II studied by solid-state NMR spectroscopy, J. Am. Chem. Soc. 141 (49) (2019) 19276–19288, https://doi.org/10.1021/jacs.9b05311.
[19] S.Z. Fisher, C.M. Maupin, M. Budayova-Spano, L. Govindasamy, C. Tu, M. Agbandje-McKenna, D.N. Silverman, G.A. Voth, R. McKenna, Atomic crystal and molecular dynamics simulation structures of human carbonic anhydrase II: insights into the proton transfer mechanism, Biochemistry 46 (11) (2007) 2930–2937, https://doi.org/10.1021/bi062066y.
[20] V.M. Krishnamurthy, G.K. Kaufman, A.R. Urbach, I. Gitlin, K.L. Gudiksen, D. B. Weibel, G.M. Whitesides, Carbonic anhydrase as a model for biophysical and physical-organic studies of proteins and Protein−Ligand binding, Chem. Rev. 108 (3) (2008) 946–1051, https://doi.org/10.1021/cr050262p.
[21] F. Carta, A. Akdemir, A. Scozzafava, E. Masini, C.T. Supuran, Xanthates and trithiocarbonates strongly inhibit carbonic anhydrases and show antiglaucoma effects in vivo, J. Med. Chem. 56 (11) (2013) 4691–4700, https://doi.org/10.1021/jm400414j.
[22] S. Ghorai, S. Pulya, K. Ghosh, P. Panda, B. Ghosh, S. Gayen, Structure-activity relationship of human carbonic anhydrase-II inhibitors: detailed insight for future development as anti-glaucoma agents, Bioorg. Chem. 95 (2020) 103557, https://doi.org/10.1016/j.bioorg.2019.103557.
[23] A. Scozzafava, C.T. Supuran, Glaucoma and the applications of carbonic anhydrase inhibitors, in: S.C. Frost, R. McKenna (Eds.), Carbonic Anhydrase: Mechanism, Regulation, Links to Disease, and Industrial Applications, Springer Netherlands, Dordrecht, 2014, pp. 349–359.
[24] R. Hazin, A.M. Hendrick, M.Y. Kahook, Primary open-angle glaucoma: diagnostic approaches and management, J. Natl. Med. Assoc. 101 (1) (2009) 46–50, https://doi.org/10.1016/S0027-9684(15)30811-7.
[25] G. Provensi, A. Nocentini, M.B. Passani, P. Blandina, C.T. Supuran, Activation of carbonic anhydrase isoforms involved in modulation of emotional memory and cognitive disorders with histamine agonists, antagonists and derivatives, J. Enzyme Inhib. Med. Chem. 36 (1) (2021) 719–726, https://doi.org/10.1080/14756366.2021.1891051.
[26] A. Nocentini, W.A. Donald, C.T. Supuran, Chapter 8 - human carbonic anhydrases: tissue distribution, physiological role, and druggability, in: C.T. Supuran, A. Nocentini (Eds.), Carbonic Anhydrases, Academic Press2019, pp. 151-185.
[27] P. Blandina, G. Provensi, M.B. Passani, C. Capasso, C.T. Supuran, Carbonic anhydrase modulation of emotional memory. Implications for the treatment of cognitive disorders, J. Enzyme Inhib. Med. Chem. 35 (1) (2020) 1206–1214, https://doi.org/10.1080/14756366.2020.1766455.
[28] C.T. Supuran, Acetazolamide for the treatment of idiopathic intracranial hypertension, Expert Rev. Neurother. 15 (8) (2015) 851–856, https://doi.org/10.1586/14737175.2015.1066675.
[29] C.T. Supuran, Carbonic anhydrase inhibition and the management of neuropathic pain, Expert Rev. Neurother. 16 (8) (2016) 961–968, https://doi.org/10.1080/14737175.2016.1193009.
[30] J.-Y. Winum, M. Rami, A. Scozzafava, J.-L. Montero, C. Supuran, Carbonic anhydrase IX: a new druggable target for the design of antitumor agents, Med. Res. Rev. 28 (3) (2008) 445–463, https://doi.org/10.1002/med.20112.
[31] K. Horie, K. Kawakami, Y. Fujita, M. Sugaya, K. Kameyama, K. Mizutani, T. Deguchi, M. Ito, Exosomes expressing carbonic anhydrase 9 promote angiogenesis, Biochem. Biophys. Res. Commun. 492 (3) (2017) 356–361, https://doi.org/10.1016/j.bbrc.2017.08.107.
[32] S. Bekku, H. Mochizuki, T. Yamamoto, H. Ueno, E. Takayama, T. Tadakuma, Expression of carbonic anhydrase I or II and correlation to clinical aspects of colorectal cancer, Hepat. Gastroentero. 47 (34) (2000) 998–1001.

[33] J. Pichake, P.S. Kharkar, M. Ceruso, C.T. Supuran, M.P. Toraskar, Carbonic anhydrase inhibitors: design, synthesis, and biological evaluation of novel sulfonyl semicarbazide derivatives, ACS Med. Chem. Lett. 5 (7) (2014) 793–796, https://doi.org/10.1021/ml500140t.
[34] M. Kciuk, A. Gielecińska, S. Mujwar, M. Mojzych, B. Marciniak, R. Drozda, R. Kontek, Targeting carbonic anhydrase IX and XII isoforms with small molecule inhibitors and monoclonal antibodies, J. Enzyme Inhib. Med. Chem. 37 (1) (2022) 1278–1298, https://doi.org/10.1080/14756366.2022.2052868.
[35] K.A. Poulsen, E.C. Andersen, C.F. Hansen, T.K. Klausen, C. Hougaard, I.H. Lambert, E.K. Hoffmann, Deregulation of apoptotic volume decrease and ionic movements in multidrug-resistant tumor cells: role of chloride channels, Am. J. Physiol.-Cell Physiol. 298 (1) (2010) C14–C25, https://doi.org/10.1152/ajpcell.00654.2008.
[36] C.M. Dias, H. Li, H. Valkenier, L.E. Karagiannidis, P.A. Gale, D.N. Sheppard, A. P. Davis, Anion transport by ortho-phenylene bis-ureas across cell and vesicle membranes, Org. Biomol. Chem. 16 (7) (2018) 1083–1087, https://doi.org/10.1039/C7OB02787G.
[37] N. Akhtar, A. Saha, V. Kumar, N. Pradhan, S. Panda, S. Morla, S. Kumar, D. Manna, Diphenylethylenediamine-based potent anionophores: transmembrane chloride ion transport and apoptosis inducing activities, ACS Appl. Mater. Interfaces 10 (40) (2018) 33803–33813, https://doi.org/10.1021/acsami.8b06664.
[38] T. Saha, M.S. Hossain, D. Saha, M. Lahiri, P. Talukdar, Chloride-mediated apoptosis-inducing activity of bis(sulfonamide) anionophores, J. Am. Chem. Soc. 138 (24) (2016) 7558–7567, https://doi.org/10.1021/jacs.6b01723.
[39] S. Pérez, P. Eichhorn, D.S. Aga, Evaluating the biodegradability of sulfamethazine, sulfamethoxazole, sulfathiazole, and trimethoprim at different stages of sewage treatment, Environ. Toxicol. Chem. 24 (6) (2005) 1361–1367, https://doi.org/10.1897/04-211R.1.
[40] Y.-q. Gao, N.-y. Gao, Y. Deng, Y.-q. Yang, Y. Ma, Ultraviolet (UV) light-activated persulfate oxidation of sulfamethazine in water, Chem. Eng. J. 195–196 (2012) 248–253, https://doi.org/10.1016/j.cej.2012.04.084.
[41] N.A. Littlefield, W.G. Sheldon, R. Allen, D.W. Gaylor, Chronic toxicity/carcinogenicity studies of sulphamethazine in Fischer 344/N rats: two-generation exposure, Food Chem. Toxicol. 28 (3) (1990) 157–167, https://doi.org/10.1016/0278-6915(90)90004-7.
[42] A. Hamad, M. Abbas Khan, I. Ahmad, A. Imran, R. Khalil, T. Al-Adhami, K. Miraz Rahman, Quratulain, N. Zahra, Z. Shafiq, Probing sulphamethazine and sulphamethoxazole based Schiff bases as urease inhibitors; synthesis, characterization, molecular docking and ADME evaluation, Bioorg. Chem. 105 (2020) 104336, https://doi.org/10.1016/j.bioorg.2020.104336.
[43] K.M. Doretto, L.M. Peruchi, S. Rath, Sorption and desorption of sulfadimethoxine, sulfaquinoxaline and sulfamethazine antimicrobials in Brazilian soils, Sci. Total Environ. 476–477 (2014) 406–414, https://doi.org/10.1016/j.scitotenv.2014.01.024.
[44] L. Yu, Y. Wang, X. Su, Y. Fu, F. Ma, H. Guo, Biodiversity, isolation and genome analysis of sulfamethazine-degrading bacteria using high-throughput analysis, Bioprocess Biosyst. Eng. 43 (8) (2020) 1521–1531, https://doi.org/10.1007/s00449-020-02345-1.
[45] J. Wang, W. Ben, Y. Zhang, M. Yang, Z. Qiang, Effects of thermophilic composting on oxytetracycline, sulfamethazine, and their corresponding resistance genes in swine manure, Environ. Sci. Process. Imp. 17 (9) (2015) 1654–1660, https://doi.org/10.1039/C5EM00132C.
[46] K.R. Mitchell, D. Warshawsky, Xenobiotic inducible regions of the human arylamine N-acetyltransferase 1 and 2 genes, Toxicol. Lett. 139 (1) (2003) 11–23, https://doi.org/10.1016/S0378-4274(02)00437-X.
[47] A.C.F. de Lyra, A.L. dos Santos Silva, E.C.L. dos Santos, A.M.Q. López, J.C.S. da Silva, I.M. Figueiredo, J.C.C. Santos, Molecular interaction of sulfonamides and ovalbumin, an allergenic egg protein, exploring biophysical, theoretical and biological studies, Spectrochim. Acta, Part A 228 (2020) 117747, https://doi.org/10.1016/j.saa.2019.117747.
[48] C. Türkeş, S. Akocak, M. Işık, N. Lolak, P. Taslimi, M. Durgun, İ. Gülçin, Y. Budak, Ş. Beydemir, Novel inhibitors with sulfamethazine backbone: synthesis and biological study of multi-target cholinesterases and α-glucosidase inhibitors, J. Biomol. Struct. Dyn. 40 (19) (2022) 8752–8764, https://doi.org/10.1080/07391102.2021.1916599.
[49] N. Lolak, S. Akocak, M. Durgun, H.E. Duran, A. Necip, C. Türkeş, M. Işık, Ş. Beydemir, Novel bis-ureido-substituted sulfaguanidines and sulfisoxazoles as carbonic anhydrase and acetylcholinesterase inhibitors, Mol. Diversity 27 (4) (2023) 1735–1749, https://doi.org/10.1007/s11030-022-10527-0.
[50] N. Lolak, S. Akocak, S. Bua, M. Koca, C.T. Supuran, Design and synthesis of novel 1,3-diaryltriazene-substituted sulfonamides as potent and selective carbonic anhydrase II inhibitors, Bioorg. Chem. 77 (2018) 542–547, https://doi.org/10.1016/j.bioorg.2018.02.015.
[51] S. Akocak, N. Lolak, S. Bua, C.T. Supuran, Discovery of novel 1,3-diaryltriazene sulfonamides as carbonic anhydrase I, II, VII, and IX inhibitors, J. Enzyme Inhib. Med. Chem. 33 (1) (2018) 1575–1580, https://doi.org/10.1080/14756366.2018.1515933.
[52] J.A. Verpoorte, S. Mehta, J.T. Edsall, Esterase activities of human carbonic anhydrases B and C, J. Biol. Chem. 242 (18) (1967) 4221–4229, https://doi.org/10.1016/S0021-9258(18)95800-X.
[53] M. al-Rashida, S. Hussain, M. Hamayoun, A. Altaf, J. Iqbal, Sulfa drugs as inhibitors of carbonic anhydrase: new targets for the old drugs, BioMed Res. Int. 2014 (2014) 162928, https://doi.org/10.1155/2014/162928.
[54] C.T. Supuran, Carbonic anhydrases: novel therapeutic applications for inhibitors and activators, Nat. Rev. Drug Discovery 7 (2) (2008) 168–181, https://doi.org/10.1038/nrd2467.
[55] C.A. Lipinski, F. Lombardo, B.W. Dominy, P.J. Feeney, Experimental and computational approaches to estimate solubility and permeability in drug discovery and development settings, Adv. Drug Delivery Rev. 23 (1) (1997) 3–25, https://doi.org/10.1016/S0169-409X(96)00423-1.
[56] K.A. Johnson, R.S. Goody, The original Michaelis constant: translation of the 1913 michaelis–menten paper, Biochemistry 50 (39) (2011) 8264–8269, https://doi.org/10.1021/bi201284u.
[57] H. Lineweaver, D. Burk, The determination of enzyme dissociation constants, J. Am. Chem. Soc. 56 (3) (1934) 658–666, https://doi.org/10.1021/ja01318a036.
[58] Y. Demir, The behaviour of some antihypertension drugs on human serum paraoxonase-1: an important protector enzyme against atherosclerosis, J. Pharm. Pharmacol. 71 (10) (2019) 1576–1583, https://doi.org/10.1111/jphp.13144.
[59] C. Türkeş, Carbonic anhydrase inhibition by antiviral drugs in vitro and in silico, J. Mol. Recognit. 36 (12) (2023) e3063, https://doi.org/10.1002/jmr.3063.
[60] C. Türkeş, Aldose reductase with quinolone antibiotics interaction: in vitro and in silico approach of its relationship with diabetic complications, Arch. Biochem. Biophys. 761 (2024) 110161, https://doi.org/10.1016/j.abb.2024.110161.
[61] S. Chakravarty, K.K. Kannan, Drug-protein interactions: refined structures of three sulfonamide drug complexes of human carbonic anhydrase I enzyme, J. Mol. Biol. 243 (2) (1994) 298–309, https://doi.org/10.1006/jmbi.1994.1655.
[62] K.H. Sippel, A.H. Robbins, J. Domsic, C. Genis, M. Agbandje-McKenna, R. McKenna, High-resolution structure of human carbonic anhydrase II complexed with acetazolamide reveals insights into inhibitor drug design, Acta Crystallogr., Sect. F 65 (10) (2009) 992–995, https://doi.org/10.1107/S1744309109036665.
[63] G. Madhavi Sastry, M. Adzhigirey, T. Day, R. Annabhimoju, W. Sherman, Protein and ligand preparation: parameters, protocols, and influence on virtual screening enrichments, J. Comput. Aided Mol. Des. 27 (3) (2013) 221–234, https://doi.org/10.1007/s10822-013-9644-8.
[64] V. Krivovicheva, A. Bubyrev, S. Kalinin, D. Dar'in, M. Gureev, V. Burianova, D. Vullo, M. Krasavin, C.T. Supuran, Versatile diazomethane sulfonamide for expedited exploration of azole-based carbonic anhydrase inhibitors via [3+2] cycloaddition, ChemMedChem 18 (10) (2023) e202200607, https://doi.org/10.1002/cmdc.202200607.
[65] Y. Demir, Naphthoquinones, benzoquinones, and anthraquinones: molecular docking, ADME and inhibition studies on human serum paraoxonase-1 associated with cardiovascular diseases, Drug Dev. Res. 81 (5) (2020) 628–636, https://doi.org/10.1002/ddr.21667.
[66] J.C. Shelley, A. Cholleti, L.L. Frye, J.R. Greenwood, M.R. Timlin, M. Uchimaya, Epik: a software program for pKaprediction and protonation state generation for drug-like molecules, J. Comput. Aided Mol. Des. 21 (12) (2007) 681–691, https://doi.org/10.1007/s10822-007-9133-z.
[67] T.A. Halgren, Identifying and characterizing binding sites and assessing druggability, J. Chem. Inf. Model. 49 (2) (2009) 377–389, https://doi.org/10.1021/ci800324m.
[68] R.A. Friesner, J.L. Banks, R.B. Murphy, T.A. Halgren, J.J. Klicic, D.T. Mainz, M. P. Repasky, E.H. Knoll, M. Shelley, J.K. Perry, D.E. Shaw, P. Francis, P.S. Shenkin, Glide: a new approach for rapid, accurate docking and scoring. 1. Method and assessment of docking accuracy, J. Med. Chem. 47 (7) (2004) 1739–1749, https://doi.org/10.1021/jm0306430.
[69] T.A. Halgren, R.B. Murphy, R.A. Friesner, H.S. Beard, L.L. Frye, W.T. Pollard, J. L. Banks, Glide: a new approach for rapid, accurate docking and scoring. 2. Enrichment factors in database screening, J. Med. Chem. 47 (7) (2004) 1750–1759, https://doi.org/10.1021/jm030644s.
[70] E. Margulis, A. Dagan-Wiener, R.S. Ives, S. Jaffari, K. Siems, M.Y. Niv, Intense bitterness of molecules: machine learning for expediting drug discovery, Comput. Struct. Biotech. J. 19 (2021) 568–576, https://doi.org/10.1016/j.csbj.2020.12.030.